ARTICLE NO. 79-4105

Similarities of Turbulence Structure in a Conical Diffuser with Other Wall-Bounded Flows

R. S. Azad* and R. H. Hummel†
The University of Manitoba, Winnipeg, Manitoba, Canada

Experiments were conducted in a conical diffuser with a total divergence angle of 8 deg and an area ratio of 4:1 with fully developed turbulent pipe flow at entry. The results of previous research have shown that diffuser flow can be separated into two regions, i.e., the wall region where u^2 varies linearly with distance from the wall and an inner core region starting where u reached a maximum. Detailed experiments were performed to show the similarities of diffuser flow with boundary-layer flow (and pipe flow). Such flows have recently been thoroughly researched with the aid of flow visualization. The probability density of instantaneous velocity, the behavior of the ejection, sweep, wallward and outward interaction events, and the highly intermittent nature of the fine structure near the wall in the diffuser flow are similar to the flows in other wall-bounded flows, e.g., pipe, channel, and boundary-layer flows. Measurements of fine structure parameters such as the spectra of $(\partial u/\partial t)^2$ also show that in the wall region for the diffuser the spectra have a dual slope similar to that shown by Ueda and Hinze, clearly suggesting structure similarity.

Nomenclature

A = constant that depends on macrostructure of turbulence in Eq. (1)
e = electrical signal
$F.F.$ = flatness factor
f = frequency, Hz
Δf = bandwidth
f_k = Kolmogorov frequency defined by $\bar{U}/2\pi\eta$
f_m = midband frequency
k = wave number
ℓ = sensitive length of the hot-wire
L_f = longitudinal integral scale defined by Eq. (5)
L_g = transverse integral scale defined by Eq. (6)
P = pressure
R = distance from the axis of the diffuser
R_{ref} = radius of the pipe, equal 5.08 cm
Re = Reynolds number defined by $\bar{U}_c\, 2R_{\text{ref}}/\nu$
R_λ = turbulence Reynolds number defined by $u'\,\lambda/\nu$
R_{ll} = correlation function for u fluctuation
r = distance parallel or normal to a component of fluctuating velocity
S = skewness
t = time
U = instantaneous streamwise velocity
$\bar{U}_c$ = mean velocity at the center of the pipe
u,v,w = velocity fluctuation along rectangular Cartesian coordinates x, y, and z, respectively
u^* = friction velocity
v_η = Kolmogorov velocity defined by $(\nu\bar{\epsilon})^{1/4}$
$-\overline{uv}$ = mean Reynolds shear stress per unit mass of a fluid
x or x_1 = distance along the axis of the diffuser
x_2 = radial distance, normal to the axis of the diffuser
y = distance normal to the surface
y^+ = nondimensional distance denoted by u^*y/ν
γ = intermittency factor, relative time spent by a fixed probe in turbulent fluid
$\bar{\epsilon}$ = rate of dissipation of turbulent energy per unit mass of fluid
η = Kolmogorov length scale defined by Eq. (4)
λ = Taylor microscale defined by Eq. (2)
μ = universal constant given in Eq. (1)
ν = kinematic viscosity
ρ = density of fluid
σ^2 = variance, defined by Eq. (1)

Operators

$\overline{(\ )}$ = time mean
$(\ )'$ $\equiv\sqrt{\overline{(\ )^2}}$ = root mean square

Received Oct. 31, 1978; revision received Feb. 26, 1979.

Index categories: Airbreathing Propulsion; Boundary Layers and Convective Heat Transfer—Turbulent; Nozzle and Channel Flow.

*Professor of Mechanical Engineering, Dept. of Mechanical Engineering. Member AIAA.

†Research Associate, Dept. of Mechanical Engineering. Presently with General Electric Medical Systems, Saskatoon, Canada.

Introduction

RECENT turbulence research has devoted much effort toward the investigation of wall-bounded flows, characterized by large-scale, random, intermittent inflows and outflows near the wall and the fully developed flows with large Reynolds number where the assumption of local isotropy greatly simplifies the theory. Progress in understanding the wall-bounded flows has been greatly enhanced by the use of modern flow visualization techniques pioneered by Kline, Brodkey, and others while the large Reynolds number flows have usually been studied in atmospheric surface layers using hot-wire and sonic anemometers.

In the present work the detailed statistical properties of turbulence in an 8-deg conical diffuser are explored with two basic aims. First, since the diffuser is an axisymmetric wall-bounded flow it will have many properties in common with pipe and other wall-bounded flows, the properties of which are already well documented in the literature. It is therefore interesting and useful to see how the properties of the diffuser with its adverse pressure gradient compare with the wall-bounded flows which have zero or favorable pressure gradient.

The second aim is to make measurements of the small-scale properties and compare the results with those obtained in wall-bounded flows. The existence of power law relationships for energy spectra with slopes very similar to those predicted by Kolmogorov would suggest that an inertial subrange does

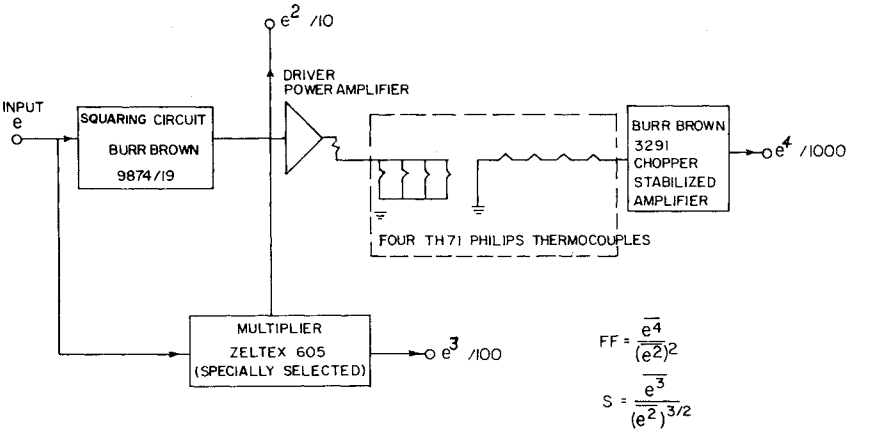

Fig. 1 Block diagram of circuit for measurement of skewness and flatness factor.

Table 1 Distribution of various flow parameters at station 30 for $Re = 137{,}000$[a]

R/R_{ref}	$\bar{U}$, m/s	u', m/s	λ, mm	R_λ	$\bar{\epsilon}$ $(cm^2/s^3)\times 10^4$	η, mm	f_k, kHz	L_f, mm	L_g, mm	L_f/L_g	L_f/η
0.0	15.4	0.96	3.52	211	17.9	0.123	19.9	43.0	7.9	5.44	350
0.236	15.1	1.17	3.84	281	22.3	0.116	20.7	51.2	10.3	4.97	441
0.433	14.3	1.48	3.78	350	36.8	0.103	22.1	46.5	12.2	3.81	451
0.630	12.5	1.97	3.88	478	61.9	0.090	22.1	72.9	13.6	5.36	810
0.827	10.2	2.38	3.57	531	106.7	0.079	20.5	64.1	14.0	4.58	811
1.024	7.7	2.51	3.04	477	163.6	0.071	17.3	57.6	14.0	4.11	811
1.220	5.4	2.35	2.54	373	205.4	0.067	12.8	40.4	12.2	3.31	603
1.398	3.3	1.79	1.90	213	213.0	0.066	8.0	27.3	9.8	2.79	414
1.496	2.6	1.53	1.89	181	157.3	0.071	5.8	22.3	9.3	2.40	314

[a]Station 30 is 30 cm from the exit of the diffuser. R = distance from the axis of the diffuser in cm; wall is located at $R = 8$ cm.

exist in a diffuser flow and that the similarity theories of Kolmogorov are at least partially applicable to laboratory flows at modest Reynolds numbers.

Data concerning mean velocities, turbulence intensities, correlation coefficients, and the energy budget for a diffuser have previously been given by Okuobi and Azad.[1] They postulated the existence of a "wall turbulent layer" which extends from the wall to a point of maximum u'; in this region $\overline{u^2}$ varies linearly with distance from the wall. A detailed literature survey of diffuser research up to that time was also given. Azad and Hummel[2] have shown that for the same region (which they call the "wall intermittent region") the fine structure is highly intermittent. They measured the intermittency factor γ, of $\partial^2 u/\partial y \partial t$ by using two hot-wire probes separated 1 mm in the radial direction and found γ to approach zero close to the wall.

The mechanism of turbulence in the wall region of a boundary layer has been studied in great detail by Kline, Corino, Brodkey, and others with the aid of flow visualization techniques. Willmarth[3] gives a detailed review of much of the earlier work. An important conclusion of these studies is that the disturbance mechanism consists of an inrush of high (axial) momentum fluid toward the wall alternating with low momentum fluid away from the wall. This process repeated itself in a semiorganized random, intermittent manner which has often been referred to as bursting. Some of the most useful consequences of these visual observations, as summarized by Ueda and Hinze[4] (U-H), are restated as follows:

1) Turbulence energy production is associated with, and dominated by, the intermittent inrush-ejection cycle and consequently by the large-scale turbulence.

2) The turbulence dissipation process is also strongly related to the inrush-ejection cycle because of the high local shear rates which exist between the large structures of fluid with different momentum.

A structure is conjectured as a relatively large fluid mass with length scale comparable to the integral length scale and with no large velocity gradients in its interior. Since high local shear rates result in an intense fine structure, detailed fine structure measurements are useful in understanding the underlying disturbance mechanism.

In view of the observed relatively large structures of fluids of different momentum separated by high local shear rates it is not surprising that the fine structure near a wall is very sporadically distributed in space, i.e., is highly intermittent. That this is also true to some extent for all turbulence was first observed by Batchelor and Townsend.[5] For normal variables the intermittency can be estimated by measuring the flatness factor, and using the relationship, $\gamma = 3/F.F.$ Thus, for a very intermittent signal (large intermittency) γ is small and the $F.F.$ is large. Kuo and Corrsin[6] have shown how the $F.F$ varies with R_λ for $12 < R_\lambda < 830$ in grid turbulence and jets. The overall conclusion is that the $F.F.$ (and therefore the degree of intermittency) increases with R_λ with no indication of an asymptotic maximum $F.F.$ at sufficiently high R_λ.

Kolmogorov's original theory of local isotropy and similarity postulated that the fine-scale structure is independent of the large-scale motion and that the statistical properties are uniquely determined by the kinematic viscosity ν and the average energy dissipation $\bar{\epsilon}$. The proposed cascade process did not allow for the possibility of large fluctuations in the instantaneous energy dissipation rate and was later modified by Kolmogorov[7] and Obukhov.[8] The modified theory formalized by Yaglom[9] and Gurvich and Yaglom[10] predicts that any non-negative quantity governed by fine structure has a lognormal distribution with variance given by

$$\sigma^2 = A + \mu \ell n (L_f/\eta) \tag{1}$$

Important consequences of the original theories are the existence of power laws for one-dimensional spectra and structure functions in the inertial subrange ($\eta \ll r \ll L_f$). The modified theories postulate corrections to the original

theories. These corrections are quite small and difficult to determine experimentally, especially for the lower-order structure functions. Van Atta and Chen[11] claim good agreement of the measured fourth-order structure functions with the modified theory.

An important consequence of the modified theory is that the one-dimensional energy spectra of $(\partial u/\partial x)^2$ should vary as $k^{\mu-1}$, where k is the wave number. Since these spectra are easily measured, using the Taylor frozen pattern hypothesis, estimates for μ are readily obtained. The major aim of the present work is basically twofold: 1) to show the similarity of diffuser flow with other wall-bounded flows and 2) to measure fine structure quantities such as spectra to assess the existence (and range) of an intertial subrange in diffuser flow as postulated by Kolmogorov.

Experimental Equipment and Procedure

Wind Tunnel, Diffuser, and Traversing Mechanism

The low-speed open circuit wind tunnel, the diffuser, and the traversing mechanism have been described by Azad and Hummel[2] and Okwuobi and Azad.[1] At the inlet to the diffuser the pipe flow was fully developed (see Ref. 12) and the mean and centerline velocities were 18.3 and 21.6 ms^{-1}, respectively. Mean and turbulent fields were similar to Okwuobi and Azad.[1] The kinematic pressure gradient, ρ^{-1} dP/dx, was linear and equal to 45.4 ms^{-2} at station 30. Radial position in the diffuser is given by R/R_{ref}, where R is distance from the centerline and R_{ref} the inlet radius. Axial position is given in terms of station numbers which correspond to cms measured from the exit plane.

Hot Wires, Anemometers, and Linearizers

Standard Disa hot-wire equipment included two constant-temperature anemometers 55M01, two linearizers 55D10, two 55D35 rms meters, and a 55D31 digital voltmeter. To measure the transverse integral length scale, six different hot-wire assemblies (custom-made by Disa) were used, each consisting of two independent hot wires with its own anemometer and linearizer. Wire separations (in the transverse direction) were 1, 2, 4, 6, 8, and 10 mm. The platinum-plated tungsten wires were 5 μ in diameter with an effective length, $\ell = 0.8$ mm. The ratios ℓ/η varied from 6.5 to 12. An overheat ratio of 0.8 was used. Measurements involving only a single hot wire were taken with one of the wires of the 8-mm probe. uv measurements were obtained with a Disa type 55A38 x probe.

Spectra Measurements

All spectra were measured with Kron-Hite Model 3700 filters on the smallest bandwidth ($\Delta f/f_m = 0.43$). Nearly identical results were obtained when measuring the same spectrum with both a KH 3700 filter and an HP 3590A spectrum analyzer using a bandwidth of 10 Hz. From these measurements it was concluded that the relatively large bandwidth of the KH 3700 filter did little to distort adversely the shape of the spectra.

Longitudinal Integral Length Scale, Skewness, and Flatness Factor Measurements

To measure the longitudinal integral length scale, Taylor's frozen pattern hypothesis was assumed, allowing spatial separations (in the mean flow direction) to be replaced by time separation. The required time delay was obtained by a Lyric TR 61-2 7 track analog tape recorder which has motor-driven movable playback heads allowing for continuously variable time delays up to 0.6 s. The signal-to-noise ratio of the tape recorder was measured to exceed 40 dB, with the frequency response flat from dc to 20 kHz at a tape speed of 60 in./s.

To measure the skewness and flatness factor of a signal e, the circuit shown in Fig. 1 was constructed. The two multipliers were specially selected to have a dc accuracy of better than 0.1%. The four thermocouples have their inputs connected in parallel and their outputs in series (as suggested by Kuo and Corrsin[6]) to help neutralize the different characteristics of the individual thermocouples. The chopper stabilized amplifier was selected because of the low output voltage of the thermocouples. $\overline{e^3}$ or $\overline{e^4}$ were time averaged with a specially constructed digital integrating voltmeter (DIVM), similar to that used by Eckelmann.[13] It consisted of a voltage-to-frequency converter and a counter with a variable time base normally set to 100 s for most readings. Simultaneously, the time average $\overline{e^2}$ was measured with a Disa 55D31 digital voltmeter using an averaging time of 100 s.

Intermittency and Spectra Measurements of $\partial u/\partial t$

The intermittency factor of $\partial u/\partial t$ was measured with a circuit similar to that used by Kuo and Corrsin.[6] Threshold and time delay settings were adjusted using a dual-beam storage oscilloscope to compare the output signal with the input signal. The signal $\partial u/\partial t$ was formed with a Disa 55A06 Random Signal Indicator and Correlator preceded by a four-pole low-pass filter with cutoff frequency set equal to the Kolmogorov frequency f_k. To measure the spectra of $\partial u/\partial t$ the signal was first squared with the squaring circuit of Fig. 1 and the spectra measured with a Kron-Hite filter and a Disa 55D35 rms meter.

Truncated uv Correlation Measurements

These quantities are discussed in detail by Wallace et al.[14] and were measured using a circuit similar to theirs. The nontruncated uv correlation was found to equal the algebraic sum of the truncated components within 5%.

Experimental Results

Preliminary Experiments

Because of the bulk of the proposed experiments it was decided at the outset to perform the main body of experiments only at one axial position which should be representative of developing diffuser flow and also only at one Reynolds number if Reynolds number similarity could be shown to exist. (It has been recognized that the flow is developing in the downstream direction and no single axial position is truly representative of "developing" diffuser flow.) To achieve the first goal, some statistical properties of the u fluctuations were measured to show how they evolved down the diffuser. Mean velocities and turbulence intensities have already been given by Okwuobi and Zad.[1] The values of $\bar{U}$ and u' for various radial positions at station 30 are given in Table 1. More interesting are the higher moments, i.e., skewness and flatness factor which were measured throughout. Figure 2 shows the probability density of the instantaneous velocity U for various radial positions at station 30 (30 cm from the outlet of the diffuser). On the centerline the turbulence intensity is relatively small and the distribution of U is negatively skewed. Comparing the result with Fig. 10 of Eckelmann,[13] we see a very similar type of probability density distribution near the wall of a turbulent channel flow. The negative skewness far from the wall is due to the intermittent ejection of low momentum fluid away from the wall. Moving closer to the diffuser wall at $R/R_{ref} = 1.03$, the distribution becomes symmetric, i.e., skewness is zero. The turbulence intensity, however, is very large and the flatness factor is less than 3. (Eckelmann[13] found u to have zero skewness at $y^+ = 10.6$; Ueda and Hinze[4] at $y^+ = 15$ for a zero pressure gradient boundary layer). This position also corresponds approximately to the point of maximum shear stress in Okwuobi and Azad.[1] Moving closer to the wall the skewness becomes positive (as it does in channel flow) with an increase in flatness factor.

Measurements by Okwuobi and Azad[1] show that the turbulent field has no appreciable Reynolds number

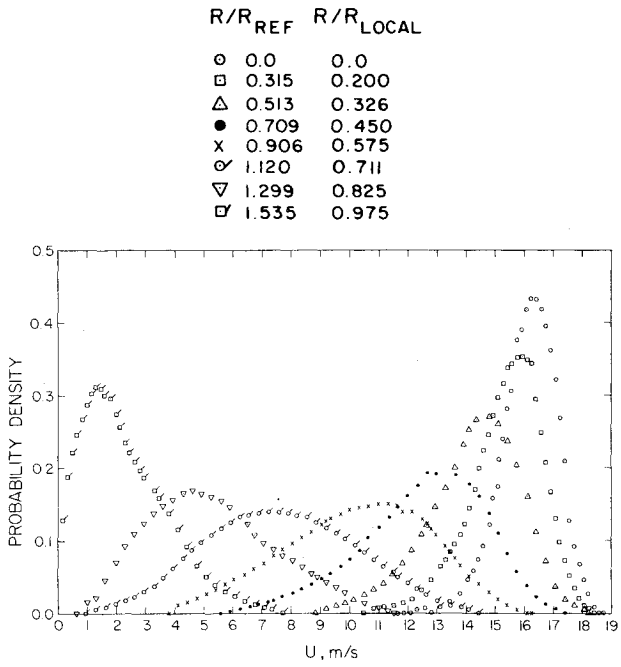

Fig. 2 Probability density distribution of the instantaneous streamwise velocity, U at station 30 for $Re = 137{,}000$.

dependence. These conclusions were based on measurements of mean velocity, fluctuating quantities, u', v', w' and shear stresses $\overline{uv}$, $\overline{uw}$. Finer details of the turbulent velocity field, involving higher moments, were considered necessary to test their conclusions. Toward this objective it was decided to measure skewness and flatness factor of u throughout the diffuser flowfield at two Reynolds numbers, $Re = 137{,}000$ and $Re = 340{,}000$. The results at station 30 are shown in Fig. 3. Flatness factor values show negligible Reynolds number dependence while skewness values are slightly lower at the higher Reynolds number. The results thus confirm that Reynolds number plays only a secondary role, and also demonstrate the symmetry of the flow.

Figures 4a and 4b show contours of isoskewness and isoflatness factor throughout the diffuser. At the inlet (fully developed pipe flow) the skewness is negative and decreasing in magnitude from the centerline to the wall. The flatness factor is slightly larger than the Gaussian value. Moving downstream, a contour of minimum flatness factor (less than 3) and a contour of zero skewness exist at approximately the pipe radius. They bulge out slightly near the center (station 30) but move back toward the centerline toward the diffuser exit. Proceeding downstream but closer to the centerline, a ridge of maximum negative skewness starts becoming more prominent. Along this ridge the flatness factor is a maximum. The ridge finally meets the centerline at station 5, 5 cm from the outlet of the diffuser. The interpretation is that as the fluid moves downstream, the effect of the large-scale motion nearer the wall ejects the low momentum fluid further toward the centerline. The ridge marks an outer limit (measured from the wall) for which this process is effective. Finally, at station 5 the large-scale motion is of such magnitude as to eject low momentum fluid all the way to the centerline. Thus from station 5 on to station 0, at the outlet of the diffuser, low momentum fluid is ejected up to and across the centerline randomly but from all radial directions due to axial symmetry. Thus, at the centerline low momentum fluid is no longer such a rare event and the skewness becomes less negative. Because of this rather dramatic change in structure near the diffuser exit, station 30 (further upstream) was selected for the more detailed experiments. To insure that no signals contained frequency components in excess of 20 kHz (the upper frequency limit of the KH 3700 filters) all further

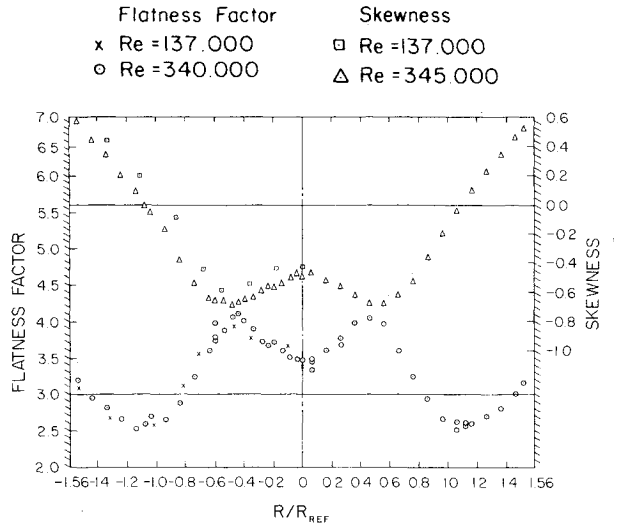

Fig. 3 Skewness and flatness factor of u at station 30.

measurements were restricted to the lower Reynolds number, $Re = 137{,}000$.

Flow Parameters—Length Scales

Kolmogorov's similarity theories on the existence of an inertial subrange require that integral length scale L_f be much larger than the Kolmogorov length scale η. It is therefore useful to measure these quantities. Taylor microscale, λ was calculated from

$$\lambda^2 = \left[\frac{\overline{u^2}}{(\partial u/\partial t)^2} \right] \bar{U}^2 \tag{2}$$

Mean dissipation $\bar{\epsilon}$ was calculated using the isotropic relationship

$$\bar{\epsilon} = 15\nu \overline{u'^2}/\lambda^2 \tag{3}$$

and η by

$$\eta = (\nu^2/\bar{\epsilon})^{1/4} \tag{4}$$

where ν is the kinematic viscosity.

These quantities are shown in Fig. 5 and tabulated in Table 1. The turbulence Reynolds number $R_\lambda = u'\lambda/\nu$ is also shown. It has a well defined peak at $R/R_{ref} \approx 0.9$, corresponding approximately to the pipe radius.

The longitudinal integral length scale L_f was calculated from

$$L_f = \int_0^\infty R_{11}(x_1, 0; 0)\, dx_1 \tag{5}$$

where R_{11} was obtained using analog time delay in conjunction with Taylor's frozen pattern hypothesis. The transverse integral length scale L_g is defined by the following integral:

$$L_g = \int_0^\infty R_{11}(0, x_2, 0; 0)\, dx_2 \tag{6}$$

where x_2 refers to the radial (transverse) direction. However, the quantity R_{11} was only measured for x_2 spacing up to 10 mm, where the correlation was still found to be substantially greater than zero; thus the complete curve would not be obtained. The measured part was found to be well approximated by an exponential function which was then assumed to describe the complete correlation function R_{11}. Thus, using the preceding integral, L_g was obtained. The values of L_f and L_g are given in Table 1.

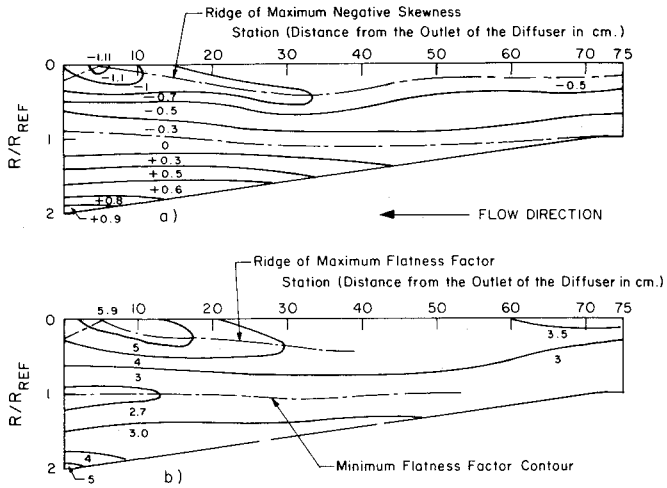

Fig. 4 Iso-skewness and flatness factor contours of u for $Re = 340{,}000$.

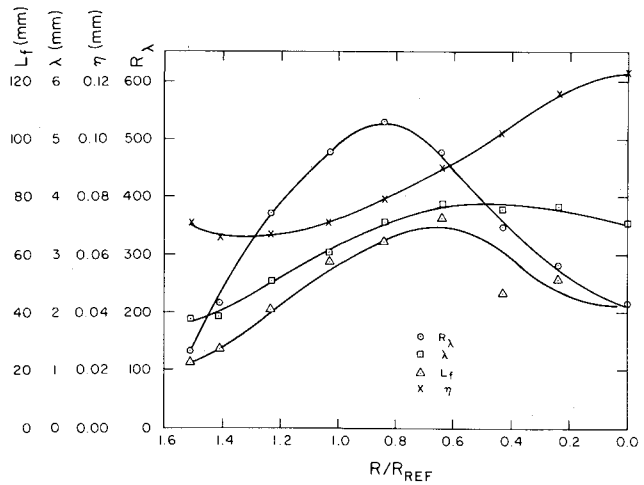

Fig. 5 Distribution of R_λ, Taylor length scale λ, longitudinal integral length scale L_f, and Kolmogorov microscale η at station 30.

Both integral scales reach a maximum at approximately $R/R_{ref} = 0.8$. The ratio of the scales varied from 5.49 (on the centerline) to 2.40 near the wall. According to Comte-Bellot and Corrsin[15] the approximate ratio $L_f/L_g = 2$ for isotropic turbulence.

Flatness Factor, Skewness, and Intermittency

The flatness factor of a random signal $e(t)$ is given by $\overline{e^4}/(\overline{e^2})^2$. Signals with low intermittency factor have a large *F.F.* The skewness S is given by $\overline{e^3}/(\overline{e^2})^{3/2}$. This is a measure of symmetry; signals with negative skewness have relatively rare large negative values (with respect to the mean) while signals with positive skewness have relatively rare large positive values. The *F.F.* of the u fluctuations after passing through a bandpass filter (with bandwidth $\Delta f/f_m = 0.43$) is shown in Fig. 6. Not surprisingly, the *F.F.* increases with increasing frequency, a universal property of all turbulence. Frequency is nondimensionalized by the Kolmogorov frequency f_k. Figure 7 shows the peak values of the *F.F.* obtained from Fig. 6 together with the intermittency factor γ of $\partial u/\partial t$. There is a clear relationship between the *F.F.* and γ. In the central core region ($R/R_{ref} < 1$) γ is unity and the maximum *F.F.* remains constant (approximately 22). Closer to the wall γ goes to zero as the maximum *F.F.* becomes very large. At the lower frequencies the *F.F.* approaches the Gaussian value of 3 but closer to the wall this becomes slightly less than 3.

In the chapter on locally isotropic turbulence, Monin and Yaglom[16] discuss the variation of the skewness S and *F.F.* of $\partial u/\partial t$ with R_λ. From this discussion S is expected to vary as $R_\lambda^{3/16}$ and *F.F.* as $R_\lambda^{1/2}$ assuming the universal constant μ of Eq. (1) to equal 0.5; although Frenkiel and Klebanoff[17] found that μ varies with the R_λ. Thus, both S and *F.F.* increase with R_λ. This has been verified by Wyngaard and Tennekes[18] for atmospheric turbulence. However, for wind-tunnel turbulence with R_λ less than 1000 the trend for S is reversed as shown in Fig. 12 of U-H. Figure 8 shows complete agreement with Fig. 12 of U-H for skewness, but the agreement is only partial for the *F.F.* In our case, the two large *F.F.* values above the line correspond to measurements made near the wall while the cluster of three values of *F.F.* for largest R_λ correspond to measurements made near the maximum shear line. Thus, complete agreement is only obtained on and near the centerline.

Spectra

Nondimensional spectra $E_u/\eta\ v_\eta^2$ vs the nondimensional wave number k_η are given in Fig. 9. Their universal character at high wave number compares favorably with the result given by Monin and Yaglom (Ref. 16, p. 491) except that our data drop off somewhat faster at the high wave numbers, presumably because our probes are nearly 10η in length. However, the effect is small with little bearing on the overall conclusion we can draw from our experiments. A useful characteristic of this type of plot is that it shows precisely how the spectrum varies with R_λ. For low R_λ the low wave number part of the spectrum drops off much faster, leaving very little spectrum with $-5/3$ slope, i.e., very little inertial subrange. Spectra of $(\partial u/\partial t)^2$ are given in Fig. 10. Before taking the time derivative, the u signal was low-pass filtered with the cutoff frequency set to the Kolmogorov frequency. Following U-H, the spectral distribution $E\phi\phi$ [where $\phi = (\partial u/\partial t)^2$] was plotted in the nondimensional form $u^{*2}E\phi\phi/2\pi\nu E_\infty$ where $E_\infty = \int_0^\infty E\phi\phi\, df$. The friction velocity u^* was measured to be 0.354 m/s. The nondimensional frequency $2\pi f\nu/u^{*2}$ was found to be almost similar to U-H.

Truncated uv Correlations

In an attempt to quantify the visualization results of Brodkey, Kline, and their co-workers, Wallace et al.[14] sorted the contributions to the uv product into four categories depending on the signs of u and v. Thus,

$$\overline{uv} = \overline{u^- v^+} + \overline{u^+ v^-} + \overline{u^+ v^+} + \overline{u^- v^-} \tag{7}$$

The four quantities on the right in Eq. (7) are referred to as the truncated uv correlations. With each is associated a particular type of event with a name inspired by the results of the visualization studies. Thus, $u^- v^+$ is nonzero when low (axial) momentum fluid is ejected away from the wall, hence the name ejection event. Similarly $u^+ v^-$ is nonzero when high (axial) momentum fluid is swept toward the wall, hence the name sweep event. Associated with the remaining two quantities, $u^+ v^+$ and $u^- v^-$, are the so-called outward and wallward interactions, respectively. Figure 11 shows truncated uv correlation measurements at station 30. The important result is that, toward the wall ($R/R_{ref} > 0.9$) sweep events are larger than ejection events, whereas toward the centerline ejection events are larger than sweep events.

Discussion of Results

The most noticeable feature of the flatness factor of the filtered signal is that its maximum value increases sharply as the wall is approached. For diffuser flow this maximum value exceeds 100 near the wall as shown in Fig. 6 and 7. The same trend has also been observed by U-H for wall-bounded flow with zero pressure gradient. For instance, U-H give a maximum value for the *F.F.* of the filtered signal of about 65 at $y^+ = 5.01$ and about 20 at $y^+ = 332$. U-H suggest that for

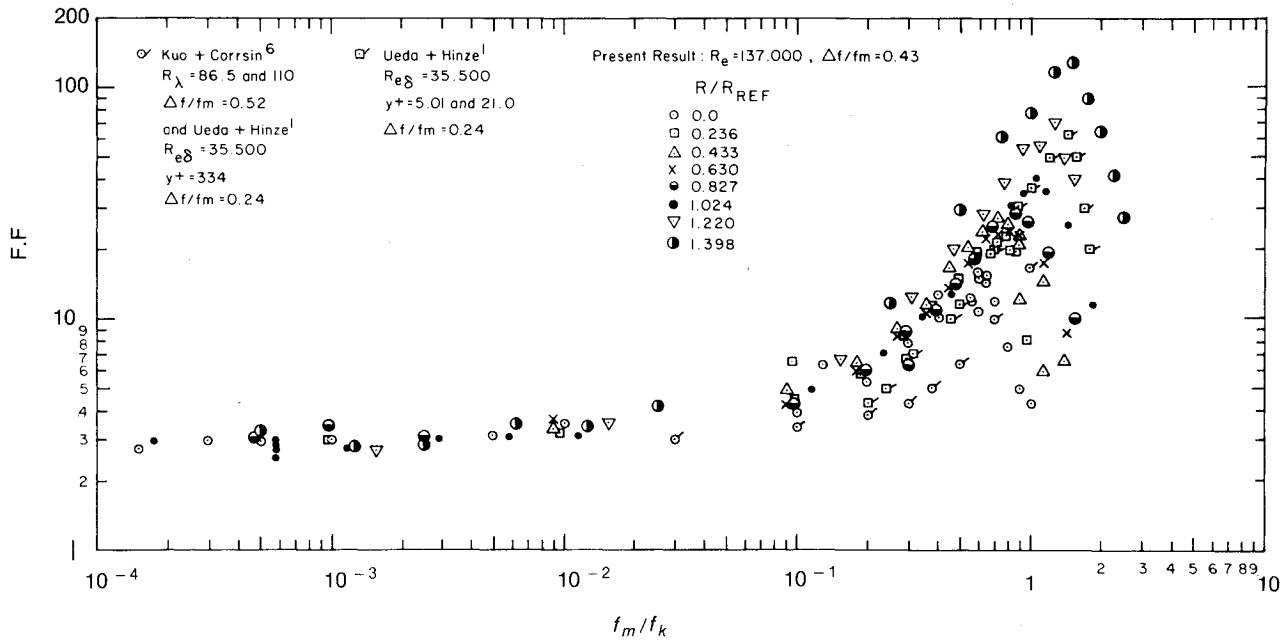

Fig. 6 Flatness factor of filtered signals of u at station 30.

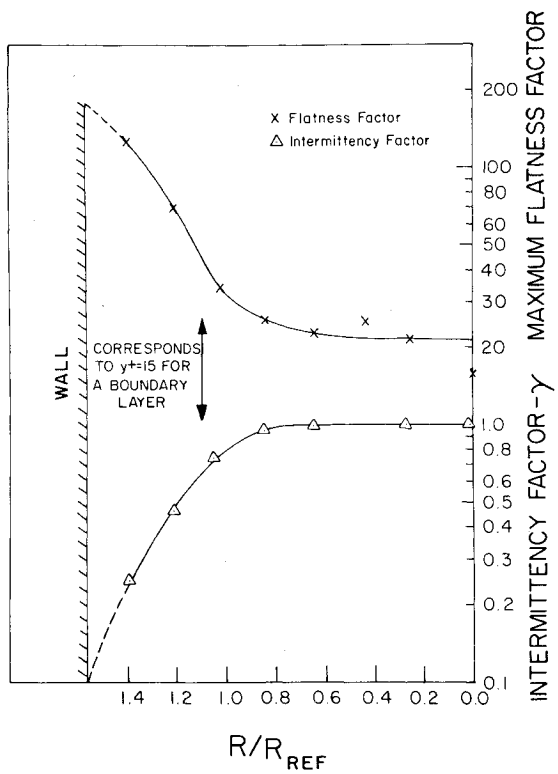

Fig. 7 Maximum flatness factor of filtered signals and intermittency factor of $(\partial u/\partial t)$ at station 30.

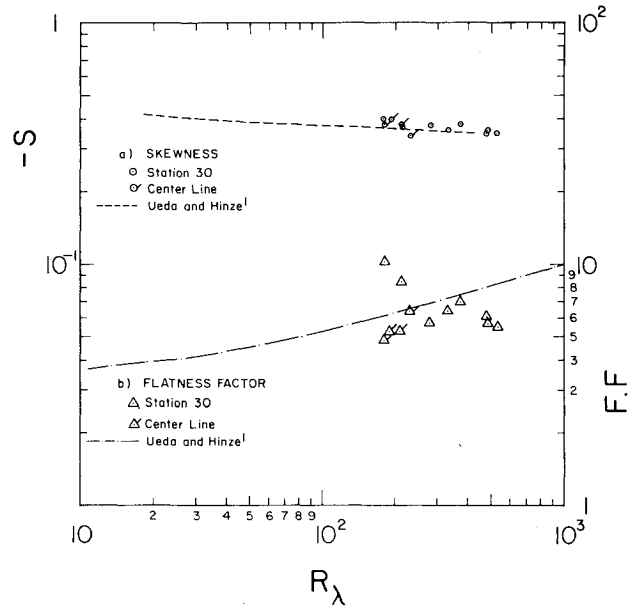

Fig. 8 Skewness and flatness factor of $(\partial u/\partial t)$ as a function of R_λ.

the boundary layer the inrush and outflow are effective far from the wall, thus doubling the spatial density of bursts which will reduce the flatness factor. Near the wall only the inrush phase will be effective, with a corresponding reduction of bursts and an increase in flatness factor. The exact nature of the flow for a boundary layer has been studied in great detail with the aid of flow visualization and much information is available on how the bursting cycle proceeds through the various phases. One cannot extrapolate these results to the case of a diffuser flow with its adverse pressure gradient. For the diffuser, however, there is also a relatively wide region $(R/R_{ref} > 1.1)$ analogous to the boundary layer with $y^+ \leq 15$ for which the intermittency of the fine structure is very large.

Figure 12 shows S and $F.F.$ of $\partial u/\partial t$ as a function of the radial position. The results for boundary-layer and pipe flow, taken from U-H and Elena,[19] respectively, are also shown. For all of these measurements the signals were first passed through a low-pass filter with cutoff set to the Kolmogorov frequency. A y^+ value of 15 in the U-H and Elena data is made to correspond to $R/R_{ref} = 1.0$, since in both cases this corresponds to the position of maximum u'. U-H give the following explanation for their data. At $y^+ < 15$ the fine structure, characterized by $\partial u/\partial t$, is influenced only by the inrush phase of the large-scale motion resulting in increased intermittency and $F.F.$ for $\partial u/\partial t$, which their result shows. Furthermore this increased $F.F.$ cannot be attributed to increased R_λ which decreases in this region as the wall is approached. Further from the wall, at $y^+ > 20$, the $F.F.$ decreases whereas R_λ remains constant. The decreasing $F.F.$

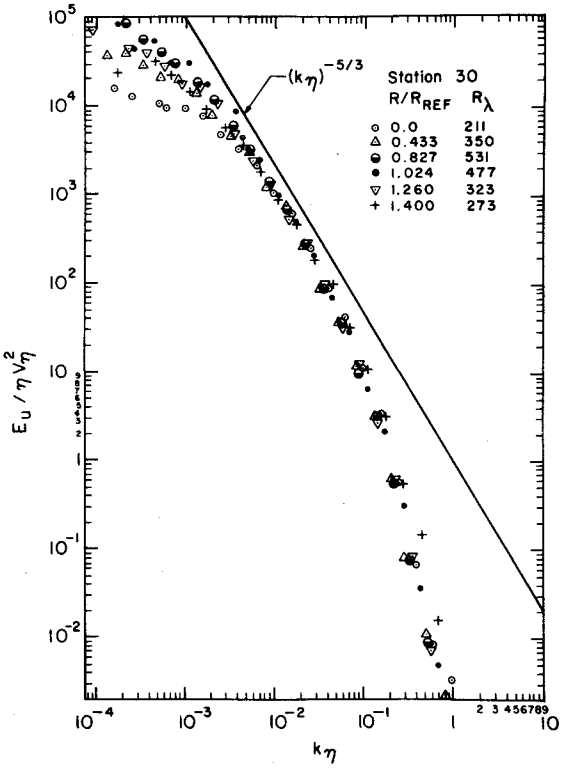

Fig. 9 Normalized one-dimensional spectra of u.

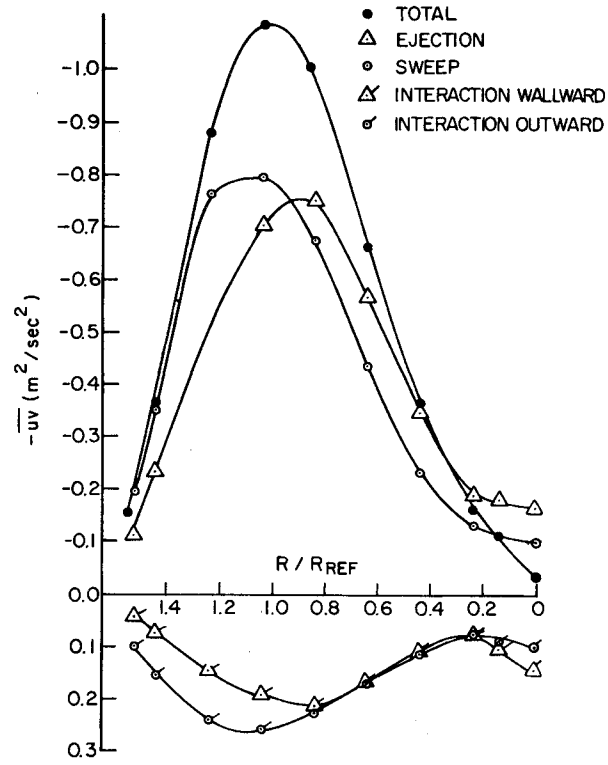

Fig. 11 Truncated uv correlations at station 30.

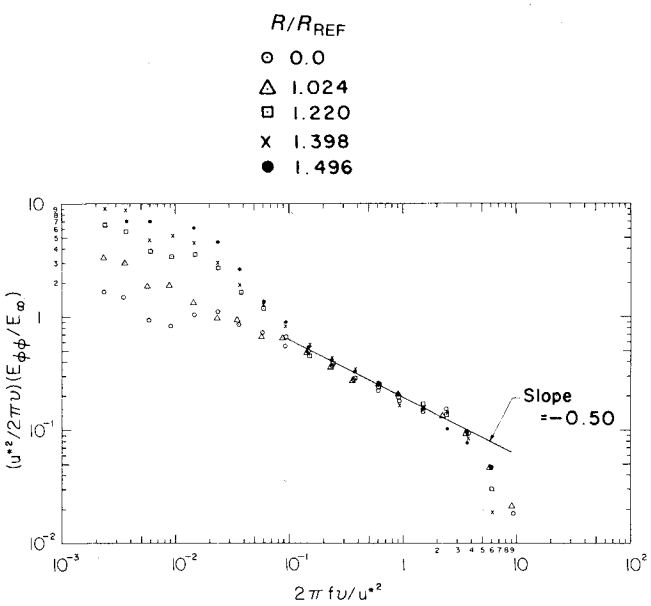

Fig. 10 Nondimensional spectra of $(\partial u/\partial t)^2$ at station 30.

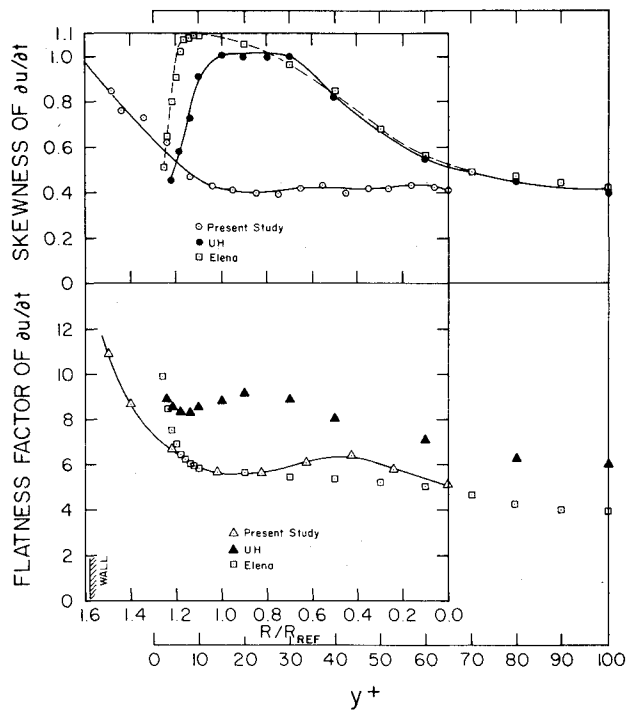

Fig. 12 Skewness and flatness factor of $(\partial u/\partial t)^2$.

is attributed to both the inrush and outflow phases of the large-scale motion. The large positive value of skewness near $y^+ = 15$ is attributed to the intermittent inrush of high momentum fluid which increase u with time but with no corresponding outflow of low momentum fluid which would tend to make the flow symmetrical, i.e., reduce the skewness. For the diffuser at $R/R_{ref} < 0.6$ the *F.F.* is approximately the same as it would be for a shear-free flow with the same R_λ. At $R/R_{ref} = 0.95$ the *F.F.* is less than the value obtained for shear-free flow with the same R_λ. No explanation is offered for this phenomenon. Wallward from $R/R_{ref} = 1.11$ the *F.F.* increases sharply, even surpassing the maximum value obtained by U-H and Elena very close to the wall. This result suggests that for this type of diffuser flow there is some similarity between the flow at $R/R_{ref} > 1.0$ and the flow at $y^+ < 15$ for a boundary-layer and pipe flow, i.e., the wall layer is much thicker. However, comparison of the skewness values for the two types of flow shows no similarity in the wall region. The skewness for the diffuser keeps increasing and does not show any tendency to decrease as this trend is evident in U-H and Elena.[19] This tendency may be because there are no measurements available very close to the wall, i.e., no measurement in the viscous sublayer.

The u spectra measurements similarly show a $-5/3$ power law over a rather restricted range which tends to diminish as the wall is approached. U-H have reported spectra measurements of $(\partial u/\partial t)^2$ in a boundary layer and have found that, in the buffer layer, the spectra have two distinct power law regions. In the lower frequency range the exponent is the same as that for the viscous sublayer while in the higher frequency range it is the same as for the outer part of the wall region; furthermore the power laws extend over a frequency range larger than just the inertial subrange as predicted by Yaglom.[9] The diffuser results, Fig. 10, are in qualitative agreement with the boundary-layer results of U-H. However, for the diffuser the high-frequency spectra collapse on to a single line with a gradient equal to 0.50. For the inner core region (corresponding to the outer region for a boundary layer) this slope is maintained at a lower frequency. Data obtained in the wall region show two slopes similar to the buffer layer of U-H. For the diffuser the slopes pertaining to low frequencies have a value of approximately 1, which is twice the value for high frequencies. In the U-H case, the slopes are -0.500 and -0.276 for lower and higher frequencies, respectively. These values of U-H are qualitatively similar to the values obtained in the diffuser flow. From this one may conjecture that the slope for the viscous sublayer in the diffuser flow would be unity.

Four events characterized by ejection ($u<0$, $v>0$), sweep ($u>0$, $v<0$), interaction wallward ($u<0$, $v<0$), and interaction outward ($u>0$, $v>0$) of truncated turbulence signals and the mean value of uv for the diffuser flow are presented in Fig. 11. The preceding characterization of the truncated signals was introduced by Wallace et al.[14] for pipe and channel flows. Following their interpretation, Fig. 11 shows that at $R/R_{ref} \approx 0.94$, associated with the maximum production of turbulent energy, the contributions of ejections and sweeps are equal and each of them has a value of about 75% of $-\overline{uv}$. At the same position, the contributions of the wallward and outward interaction roughly make up for the excess of 50% and, in turn, the net $-\overline{uv}$ is obtained as required. The sweep events become important as one moves toward the wall from this point and the ejection events are important toward the axis of the diffuser. In the wall region the outward interaction is greater than the wallward interaction, implying that accelerated regions are being driven away from the wall whereas in the core region of the diffuser the reverse is true. The results shown in Fig. 11 completely agree with Wallace et al.[14] if the $R/R_{ref} \approx 0.94$ is replaced by $y^+ = 15$. Furthermore, Grass[20] emphasized the sweep event in the wall region and this point has also been corroborated by the model and experimental results of Nakagawa and Nezu.[21]

Conclusions

As a result of the present work in an adverse pressure gradient the following conclusions can be drawn.

1) The probability distributions of the instantaneous velocity across the diffuser are similar to those of a channel flow.

2) The spectra of $(\partial u/\partial t)^2$ denote two slopes, one for the outer layer and the other for the viscous sublayer. This behavior is similar to the boundary layer with zero pressure gradient.

3) In the vicinity of $R/R_{ref} \approx 1$, the diffuser flow shows additional similarities with boundary-layer, channel, and pipe flows in the vicinity of $y^+ \approx 15$. The similarities are a) the root-mean-square of the longitudinal turbulence fluctuation attains a maximum value, and the skewness and the flatness factor of u are zero and minimum value, respectively; b) for $R/R_{ref} > 1$ and $y^+ < 15$, the skewness of u is positive with sweep events making a larger contribution to uv than ejection events; c) for $R/R_{ref} < 1$ and $y^+ > 15$, the skewness of u is negative with ejection events making a larger contribution to uv than sweep events.

The dissimilarity noted was that the maximum skewness of $(\partial u/\partial t)$ at $y^+ \approx 15$ does not occur in the diffuser at $R/R_{ref} \approx 1$.

Acknowledgment

This work was supported by the National Research Council of Canada. The authors wish to thank S. W. Greenwood, for reading the original manuscript.

References

[1] Okwuobi, P.A.C. and Azad, R. S., "Turbulence in a Conical Diffuser with Fully Developed Flow at Entry," *Journal of Fluid Mechanics*, Vol. 57, Feb. 20, 1973, pp. 603-622.

[2] Azad, R. S. and Hummel, R. H., "Measurement of the Intermittency Factor in Diffuser Flow," *Canadian Journal of Physics*, Vol. 49, Dec. 1, 1971, pp. 2917-2930.

[3] Willmarth, W. W., "Structure of Turbulence in Boundary Layers," *Advances in Applied Mechanics*, Vol. 15, Academic Press, New York, 1975, pp. 159-254.

[4] Ueda, H. and Hinze, J. O., "Fine-Structure Turbulence in the Wall Region of a Turbulent Boundary Layer," *Journal of Fluid Mechanics*, Vol. 67, Jan. 14, 1975, pp. 125-143.

[5] Batchelor, G. K. and Townsend, A. A., "The Nature of Turbulent Motion at Large Wave Number," *Proceedings of the Royal Society, London, Ser. A*, Vol. 199, Oct. 25, 1949, pp. 238-255.

[6] Kuo, A. Y. and Corrsin, S., "Experiments on Internal Intermittency and Fine-Structure Distribution Functions in Fully Turbulent Fluid," *Journal of Fluid Mechanics*, Vol. 50, Nov. 29, 1971, pp. 285-319.

[7] Kolmogorov, A. N., "A Refinement of Previous Hypotheses Concerning the Local Structure of Turbulence in a Viscous Incompressible Fluid at High Reynolds Number," *Journal of Fluid Mechanics*, Vol. 13, May 1962, pp. 82-85.

[8] Obukhov, A. M., "Some Specific Features of Atmospheric Turbulence," *Journal of Fluid Mechanics*, Vol. 13, 1962, pp. 77-81.

[9] Yaglom, A. M., "The Influence of Fluctuations in Energy Dissipation on the Shape of Turbulence Characteristics in the Inertial Interval," *Soviet Physics (Doklady)*, Vol. 11, July 1966, pp. 26-29.

[10] Gurvich, A. S. and Yaglom, A. M., "Breakdown of Eddies and Probability Distributions for Small-Scale Turbulence," *The Physics of Fluids Supplement*, Vol. 10, Sept. 1967, pp. 59-65.

[11] Van Atta, C. W. and Chen, W. Y., "Structure Functions of Turbulence in the Atmospheric Boundary Layer over the Ocean," *Journal of Fluid Mechanics*, Vol. 44, Oct. 21, 1970, pp. 145-159.

[12] Reichert, J. K. and Azad, R. S., "Non-Asymptotic Behavior of Developing Turbulent Pipe Flow," *Canadian Journal of Physics*, Vol. 54, Feb. 1976, pp. 268-278.

[13] Eckelmann, H., "The Structure of the Viscous Sublayer and the Adjacent Wall Region in a Turbulent Channel Flow," *Journal of Fluid Mechanics*, Vol. 65, Sept. 16, 1974, pp. 439-459.

[14] Wallace, J. M., Eckelmann, H., and Brodkey, R. S., "The Wall Region in Turbulent Shear Flow," *Journal of Fluid Mechanics*, Vol. 54, July 11, 1972, pp. 39-48.

[15] Comte-Bellot, G. and Corrsin, S., "Simple Eulerian Time Correlation of Full and Narrow Band Velocity Signals in Grid-Generated Isotropic Turbulence," *Journal of Fluid Mechanics*, Vol. 48, July 28, 1971, pp. 273-337.

[16] Monin, A. S. and Yaglom, A. M., *Statistical Fluid Mechanics: Mechanics of Turbulence*, Vol. 2, The MIT Press, Cambridge, Mass., 1975.

[17] Frenkel, F. N. and Klebanoff, P. S., "On the Lognormality of the Small-Scale Structure of Turbulence," *Boundary-Layer Meteorology*, Vol. 8, March 1975, pp. 173-200.

[18] Wyngaard, J. C. and Tennekes, H., "Measurements of Small-Scale Structure of Turbulence at Moderate Reynolds Numbers," *The Physics of Fluids*, Vol. 13, Aug. 1970, pp. 1962-1969.

[19] Elena, M., "Etude Experimentale de al Turbulence au Voisinage de la Paroi d'un Tube Legerement Chauffe," *International Journal of Heat and Mass Transfer*, Vol. 20, Sept. 1977, pp. 935-944.

[20] Grass, A. J., "Structural Features of Turbulent Flow over Smooth and Rough Boundaries," *Journal of Fluid Mechanics*, Vol. 50, Nov. 29, 1971, pp. 233-255.

[21] Nakagawa, H. and Nezu, I., "Prediction of the Contributions to the Reynolds Stress from Bursting Events in Open-Channel Flows," *Journal of Fluid Mechanics*, Vol. 80, April 4, 1977, pp. 99-128.